

Article

Adsorption of Zn(II), Pb(II), and Cu(II) by Residual Soil-Derived Zeolite in Single-Component and Competitive Systems

Zhe Wang *, Wen Li, Liling Wang, Yi Zhang, Jiake Li and Yuling Liu *

State Key Laboratory of Eco-Hydraulics in Northwest Arid Region of China, Xi'an University of Technology, No. 5 South Jinhua Road, Xi'an 710048, China; 2200421172@stu.xaut.edu.cn (W.L.); 2210421173@stu.xaut.edu.cn (Y.Z.); sys@xaut.edu.cn (J.L.)

* Correspondence: wangzhewater@xaut.edu.cn (Z.W.); liuyuling@xaut.edu.cn (Y.L.)

Abstract: Using construction residual soil (RS) as the raw material, RS-derived zeolite (RSDZ) was prepared through a fusion-hydrothermal process. The adsorption performance and mechanisms of RSDZ for Pb^{2+} , Zn^{2+} , and Cu^{2+} were investigated in single-component and competitive systems. The strong RSDZ X-ray diffraction peaks at $2\theta = 12.47, 17.73, 21.65, 28.18,$ and 33.44° , together with the results of scanning electron microscopy and Fourier transform-infrared spectroscopy (FT-IR) indicated that NaP1 zeolite ($\text{Na}_6\text{Al}_6\text{SiO}_{32}\cdot 12\text{H}_2\text{O}$) was successfully synthesised. The Brunauer–Emmett–Teller surface area, average pore size, and cation exchange capacity increased from $9.03 \text{ m}^2\cdot\text{g}^{-1}$, 18.85 nm , and $0.12 \text{ meq}\cdot\text{g}^{-1}$ to $47.77 \text{ m}^2\cdot\text{g}^{-1}$, 41.60 nm , and $0.61 \text{ meq}\cdot\text{g}^{-1}$, respectively, after the fusion-hydrothermal process. The maximum Langmuir adsorption capacity of RSDZ for Zn^{2+} , Pb^{2+} , and Cu^{2+} in the unary systems was $0.37, 0.38,$ and $0.40 \text{ mmol}\cdot\text{g}^{-1}$, respectively. Increasing the initial solution pH facilitated the adsorption reaction, and the adsorption performance was stable when $\text{pH} > 3$. The distribution coefficients in the binary and ternary systems indicated that RSDZ had greater affinity for Pb^{2+} and Zn^{2+} than for Cu^{2+} due to the larger ionic radius and relative atomic weight of the former two cations. The relative affinity to Pb^{2+} and Zn^{2+} was related to their concentration, with more competitive adsorption of Pb^{2+} at concentrations higher than $0.4 \text{ mmol}\cdot\text{L}^{-1}$ in binary systems and $0.25 \text{ mmol}\cdot\text{L}^{-1}$ in ternary systems. X-ray photoelectron spectroscopy and FT-IR analyses indicated that ion exchange was the main mechanism involved in the adsorption of heavy metal ions by RSDZ, accompanied by ligand exchange.

Keywords: construction residual soil; zeolite; heavy metals; competitive adsorption



Citation: Wang, Z.; Li, W.; Wang, L.; Zhang, Y.; Li, J.; Liu, Y. Adsorption of Zn(II), Pb(II), and Cu(II) by Residual Soil-Derived Zeolite in Single-Component and Competitive Systems. *Sustainability* **2023**, *15*, 13515. <https://doi.org/10.3390/su151813515>

Academic Editors: Xiaofei Tan and Jia Wen

Received: 17 July 2023

Revised: 3 September 2023

Accepted: 7 September 2023

Published: 9 September 2023



Copyright: © 2023 by the authors. Licensee MDPI, Basel, Switzerland. This article is an open access article distributed under the terms and conditions of the Creative Commons Attribution (CC BY) license (<https://creativecommons.org/licenses/by/4.0/>).

1. Introduction

The rapid development of industrial sectors, such as mineral mining and processing, fossil fuel combustion, electroplating, printing and dyeing, has contributed to the increasing discharge of wastewater containing heavy metals [1]. In 2012, $221.6 \times 10^8 \text{ m}^3$ of wastewater containing 388.4 tonnes of heavy metals was discharged by heavy metal industries in China [2]. The entry of untreated or inadequately treated heavy metal wastewater into the environment pollutes water bodies and soil. These heavy metals can eventually enter the human body via the food chain and can endanger human health [3]. Therefore, the treatment of heavy metal wastewater is a critical and urgent matter.

Treatment methods for heavy metal wastewater include membrane separation, adsorption, ion exchange, chemical precipitation, electrodialysis, and bioremediation [4]. Among the various treatment methods, adsorption has been widely employed due to its effectiveness, simple operability, and low cost [5–7]. Zeolites are a group of natural minerals consisting of an ordered arrangement of silica and alumina tetrahedra. Zeolites have often been used as heavy metal adsorbents, given their permanently negatively charged surface [8]. The use of zeolites for the treatment of heavy metal wastewater has been

extensively reported. Erdem et al. [9] studied the adsorption of various heavy metal cations by natural zeolites and ranked the adsorption capacity as $\text{Co}^{2+} > \text{Cu}^{2+} > \text{Zn}^{2+} > \text{Mn}^{2+}$. Hernández-Montoya et al. [10] showed that the excellent adsorption capacities of clinoptilolite and erionite for Pb^{2+} stemmed mainly from their strong electronegative properties, whereas the adsorption capacities for Ni^{2+} , Zn^{2+} , and Cd^{2+} were mainly influenced by their hydrated ionic radii. Modification of zeolite by acid/base/salt treatment could improve its affinity towards cationic pollutants, whereas grafting by surfactant or metallic functionalisation enabled its adsorption of anionic species [8]. However, multiple heavy metal ions often co-exist in heavy metal wastewater, and the competitive adsorption behaviour of multiple heavy metal ions on the zeolite surface has received limited attention.

Economic development has been accompanied by a growing output of residual soil (RS) from construction projects. China generated approximately $18\text{--}20 \times 10^8 \text{ m}^3$ of RS in 2017 [11]. The arbitrary piling of RS leads to the wastage of soil (rock) resources, land encroachment, and air pollution due to the production of dust [12]. Furthermore, RS may lead to geological hazards, such as landslides and mudslides [13]. Therefore, the rational disposal and resource utilisation of RS has become a top priority. The current use of RS includes the production of building materials and backfilling of cave-ins [14–16]. However, given the relatively high transport and manufacturing costs, there are challenges to promoting these low-value-added methods. Additionally, RS has a much lower content of nutrients (e.g., nitrogen, phosphorus, and potassium) than the original soil and a lower retention capacity for water and fertiliser, which makes it unsuitable as planting soil [17].

In terms of chemical composition, RS is rich in aluminosilicate minerals, such as quartz, kaolinite, and anorthite, with silicon (Si) and aluminium (Al) elements accounting for more than 50% by mass [18]. Interestingly, zeolites are also composed of Si and Al elements [8]. Thus, conversion of soil to zeolite may be possible through a series of processes to achieve the high-value-added resource utilisation of RS. A number of studies on the synthesis of zeolites using soil minerals have been reported. Wang et al. [19] reported the hydrothermal synthesis of zeolite X at 95 °C using low-grade bauxite. Garcia et al. [20] used diatomite as a Si source and $\text{Al}_2(\text{SO}_4)_3$ as an Al source to achieve the hydrothermal synthesis of zeolite Y at 100 °C. Using opal as raw material, Wu et al. [21] performed the hydrothermal synthesis of zeolite 4A at 70 °C. Yang et al. [22] established a quasi-solid-phase process at 100 °C for the synthesis of zeolite Y and A using kaolin. Liu et al. [23] converted the aluminosilicate mineral, rectorite, to zeolite P through calcination at 1000 °C. However, current research is biased towards the use of single soil minerals for the synthesis of zeolites, with limited research on the use of actual soil.

In the present study, RS was used as raw material to produce an RS-derived zeolite (RSDZ) through a fusion and hydrothermal process, followed by the characterisation of its chemical composition, crystal structure and surface properties. The adsorption capacity and pH effect on the adsorption of RSDZ in the unary system for three heavy metal ions (Zn^{2+} , Pb^{2+} , and Cu^{2+}) were determined. These metals are commonly found in wastewater from lead-zinc (Pb-Zn) ore mining and processing. The competitive adsorption behaviour of the three heavy metal ions on the RSDZ surface was also investigated in binary and ternary systems. Finally, the adsorption mechanism of RSDZ for the three heavy metal ions was characterised using X-ray photoelectron spectroscopy (XPS) and Fourier transform-infrared spectroscopy (FT-IR).

2. Materials and Methods

2.1. Experimental Reagents

Cu, Pb, and Zn standard solutions ($1000 \mu\text{g}\cdot\text{mL}^{-1}$) were purchased from the National Centre of Analysis and Testing for Non-ferrous Metals and Electronic Materials, Beijing, China. All chemical reagents were purchased from Sinopharm Chemical Reagent Co., Ltd. (Shanghai, China) and were of analytical grade.

2.2. Preparation of RSDZ

RS was obtained from a construction site in Xi'an, Shaanxi, China (34°13'34.95" N, 108°39'57.672" E). The RS sample was in a powdered form and was mainly composed of Si-, Al-, and Ca-containing minerals, such as quartz, anorthite, calcium carbonate, and kaolinite (see details in Section 3.1). Prior to the experiment, RS was air-dried, ground, passed through an 80-mesh sieve and set aside in polythene bags. The preparation parameters of RSDZ were optimised according to pre-experimental results. Specifically, 5 g of RS was placed in a nickel crucible with 4 g of NaOH. The mixture was transferred to a muffle furnace for fusion at 550 °C for 1 h to obtain the RS fusion product (RSFP). The RSFP was ground and placed in a reaction kettle with 50 mL of deionised water for a hydrothermal reaction at a reaction temperature of 95 °C and a reaction time of 12 h. At the end of the reaction, the product was centrifuged at 3000 rpm for 10 min, and the supernatant was discarded. The product was dried, ground and passed through an 80-mesh sieve. The resulting RSDZ was placed in polyethylene bottles.

2.3. Characterisation of RSDZ

The crystal structure of RSDZ was analysed by X-ray diffraction (XRD; SmartLab, RIKEN, Tokyo, Japan). Chemical composition was characterised using X-ray fluorescence spectrometry (XRF) using a model S8 Tiger apparatus (Bruker, Mannheim, Germany). Morphology was observed by scanning electron microscopy (SEM) using a MerlinCompact microscope (Zeiss, Jena, Germany). Functional groups were analysed by FT-IR using a VERTEX70TGA-IR (Bruker). The specific surface area was analysed using a V-Sorb2800TP BET instrument (Jinaipu Science & Technology, Beijing, China). Cation exchange capacity (CEC) was measured using hexamine cobalt (III) chloride leaching spectrophotometry [24].

2.4. Adsorption Test

RSDZ (0.1 g) was placed in a 50 mL centrifuge tube, followed by 40 mL of heavy metal solutions (including unary Zn²⁺, Pb²⁺, and Cu²⁺ solutions, binary Zn-Cu, Cu-Pb, and Zn-Pb solutions, and ternary Zn-Pb-Cu solution). The mixture was allowed to react on a shaker at 200 rpm and 25 °C for varying lengths of time. Each mixture was centrifuged at 4000 rpm for 10 min, and the supernatant was collected. Heavy metal concentrations in each supernatant were determined by atomic absorption spectrometry using a model AA-7000 device (Shimadzu, Kyoto, Japan). The adsorption capacity was calculated as:

$$q_e = \frac{(C_0 - C_e)}{m} \times V \quad (1)$$

where q_e is the equilibrium adsorption capacity (mmol·g⁻¹), C_0 and C_e are the mass concentrations of heavy metals before and after the reaction, respectively (mmol·L⁻¹), V is the volume of the solution (L), and m is the weight of RSDZ (g).

2.4.1. Adsorption Isotherms

The reaction time of the adsorption isotherms was 24 h. When determining the adsorption isotherms in the unary systems, the concentration range of all three heavy metal solutions was 0–1 mmol·L⁻¹. The binary system included three groups, Zn-Cu, Cu-Pb, and Zn-Pb; heavy metal ions in each group had the same initial concentrations (0.1, 0.2, 0.3, 0.4, and 0.5 mmol·L⁻¹). In the ternary system, the three heavy metal ions also had the same initial concentrations (0.05, 0.1, 0.15, 0.2, 0.25, 0.3, and 0.35 mmol·L⁻¹).

In the binary and ternary systems, the distribution coefficient K_d was used to determine the affinity of RSDZ for different heavy metal ions. Higher K_d values imply that the adsorbent has a stronger affinity for heavy metal ions, and vice versa. K_d was calculated as [25]:

$$K_d = \frac{(C_0 - C_e)}{mC_e} \times V \quad (2)$$

where K_d is the adsorption distribution coefficient ($\text{L}\cdot\text{kg}^{-1}$), and other parameters were the same as that in Equation (1).

2.4.2. Effect of Initial pH

Experiments on the effect of initial pH were performed in the unary systems. The concentration of Zn^{2+} , Pb^{2+} , and Cu^{2+} was $1.0 \text{ mmol}\cdot\text{L}^{-1}$, the initial pH of the solution was adjusted to 1, 2, 3, 4, 5, 6, and 7, and the reaction time was 24 h.

2.4.3. Adsorption-Desorption Experiment

In adsorption-desorption experiments, a ternary Zn-Pb-Cu solution was adopted (initial concentration of each ion was $0.1 \text{ mmol}\cdot\text{L}^{-1}$). After 24 h of adsorption, the removal rate of Zn^{2+} , Pb^{2+} , and Cu^{2+} was calculated as:

$$R = \frac{C_0 - C_e}{C_0} \times 100\% \quad (3)$$

where R is the removal rate (%), and other parameters are the same as in Equation (1).

The solid residue was washed with $2 \text{ mol}\cdot\text{L}^{-1}$ NaCl, then washed twice with deionised water and dried at 45°C for the next adsorption. The process was repeated three times.

2.5. Mechanistic Studies

RSDZ (0.1 g) was mixed with unary solutions containing $1.0 \text{ mmol}\cdot\text{L}^{-1}$ of Zn^{2+} , Pb^{2+} , and Cu^{2+} and allowed to react for 24 h. The heavy metal bearing RSDZ sample was obtained by centrifuging, washing with ultrapure water and drying at 45°C . Characterisation was performed before and after adsorption by XPS using a model K-Alpha+ device (Thermo Fisher Scientific, Waltham, MA, USA) and FT-IR. The XPS spectra were calibrated using the C1s fine spectrum (standard peak position 284.8 eV).

3. Results and Discussion

3.1. Characterisation of RSDZ

The XRD patterns of RS, RSFP, and RSDZ are shown in Figure 1. According to the results of XRD patterns and related previous studies [26–29], RS contained minerals that included quartz, anorthite, calcium carbonate, and kaolinite. After treatment with high-temperature fusion, the intensity of the characteristic peaks for quartz was significantly reduced or disappeared, while the kaolinite and anorthite peaks disappeared completely. These findings suggest that the high-temperature alkaline conditions destroyed the original mineral structure, with transformation into an amorphous form [26]. After the hydrothermal reaction, the characteristic peak of NaP1 zeolite appeared in the product spectrum, indicating the successful synthesis of zeolite using the “fusion-hydrothermal” process [27].

The chemical compositions of RS, RSFP, and RSDZ are shown in Table 1. No significant differences in the mass fractions of SiO_2 , Al_2O_3 , and CaO were evident. However, although Na_2O was under the detection limit in RS, as the Na content was normally low in soil, its mass fraction increased to 49.24% and 13.7% due to the introduction of NaOH during the synthesis process. The specific surface area of RSDZ was $47.77 \text{ m}^2\cdot\text{g}^{-1}$, which was a 5-fold increase relative to that of RS. The N_2 adsorption-desorption isotherms of RS and RSDZ are presented in Figure S1. The curves all exhibited type II nature, and the average pore size increased from 18.85 nm (RS) to 41.60 nm (RSDZ), which would benefit the diffusion and adsorption of heavy metal ions. The BET surface area also increased from $9.03 \text{ m}^2\cdot\text{g}^{-1}$ to $47.77 \text{ m}^2\cdot\text{g}^{-1}$. The CEC of RSDZ was $61.32 \text{ cmol}\cdot\text{kg}^{-1}$, which was a 6-fold increase relative to that of RS. The zeolite product synthesised by the fusion-hydrothermal treatment of RS is composed of a framework of $[\text{SiO}_4]^{4-}$ and $[\text{AlO}_4]^{3-}$ tetrahedra, in which the two form a three-dimensional network with a large number of voids and channels via the sharing of oxygen atoms [26,29]. It is this special structure that gives RSDZ a high specific surface area and CEC value [28].

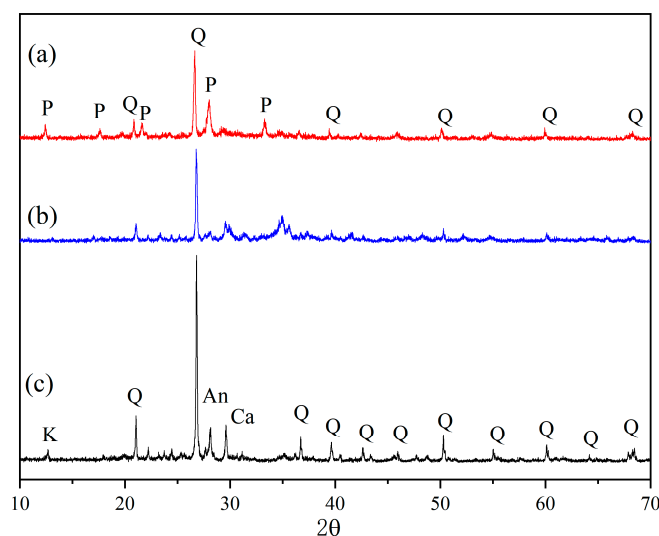


Figure 1. XRD patterns of RS (a), RSFP (b), and RSDZ (c). Q—quartz, P—NaP1 zeolite, K—kaolinite, An—anorthite, Ca—calcium carbonate.

Table 1. Chemical composition, BET surface area and CEC of RS, RSFP, and RSDZ.

Sample	SiO ₂	Al ₂ O ₃	CaO	Fe ₂ O ₃	Na ₂ O	K ₂ O	MgO	BET/(m ² ·g ⁻¹)	Average Pore Size/(nm)	CEC/(meq·g ⁻¹)
RS	58.21%	15%	10.46%	7.17%	¹	3.43%	2.65%	9.03	18.85	0.12
RSFP	30.65%	7.33%	4.97%	4.63%	49.24%	1.64%	0.53%	0.15	25.03	0.11
RSDZ	55.41%	15.8%	10.1%	0.22%	13.7%	1.78%	1.6%	47.77	41.60	0.61

¹ Not detected.

SEM images of RS, RSFP, and RSDZ are shown in Figure 2a–c. RS appeared as irregular blocks (Figure 2a) with a relatively rough surface and were mostly larger than 5 μm in size. The morphology of RSFP (Figure 2b) was very different from that of RS, with a smoother surface. The formation of this morphology was most likely related to the high-temperature calcination [29]. SEM of RSDZ (Figure 2c) revealed that particles with a microcrystalline morphology were aggregated into flocs of several μm in diameter. Comparisons with previous studies confirmed that this is a NaP1 zeolite crystal [30]. The morphology of RSDZ also explains, from a microscopic perspective, the significant increase in the specific surface area of RS after the fusion-hydrothermal treatment.

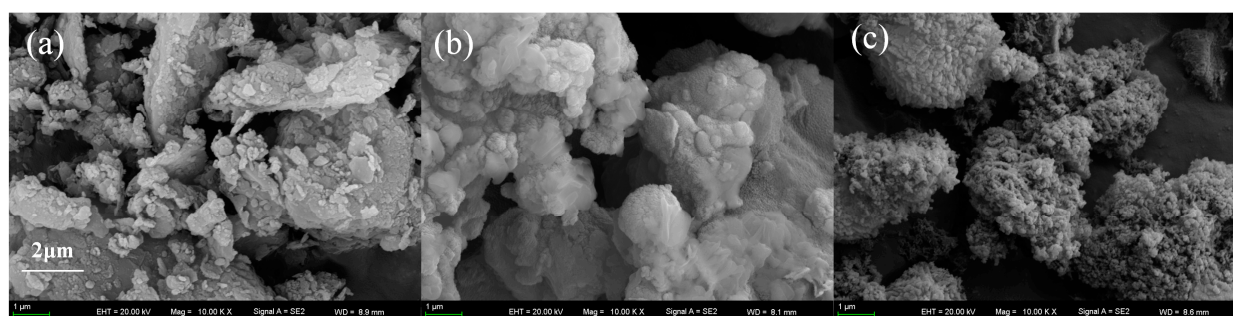


Figure 2. SEM images of RS (a), RSFP (b), and RSDZ (c).

Figure 3 shows the FT-IR spectra of RS, RSFP, and RSDZ. According to previous studies, the vibration of the aluminosilicate framework gives rise to adsorption bands in the range of 1250–400 cm⁻¹ [29]. Thus, the FT-IR spectra in this range were extracted and are presented in Figure 3. The most pronounced absorption band in the spectra was that at 1180–950 cm⁻¹, which represents the asymmetric stretching vibration of Si-O or Al-O bonds in the tetrahedral structure TO₄ (T represents Si or Al atoms) [29]. Compared to

the absorption bands in RS, the bands in RSFP and RSDZ shifted significantly towards lower wave numbers, specifically from 1030 cm^{-1} to 975 for RSFP and to 993 cm^{-1} for RSDZ. According to previous studies, this change indicates that the original Si atoms in TO_4 are replaced by Al atoms [31,32]. In the RS spectrum, the absorption band at 471 cm^{-1} shifted to 466 and 448 cm^{-1} after the reaction, which also indicated that the silicate mineral, quartz, in RS was gradually converted to the aluminosilicate mineral, NaP1 zeolite, after the reaction [29]. The absorption band in RS located at 874 cm^{-1} originated from the bending vibration of the OH groups in the layered structure of illite and kaolinite [33]. After fusion and hydrothermal crystallisation, this absorption band was weakened or even disappeared. The absorption bands at 527 and 692 cm^{-1} were related to the Al-O bond vibrations of alumina octahedra in kaolinite [33], both of which also disappeared in RSFP and RSDZ. Taken together, these findings suggest that the synthesis process destroyed the original mineral crystal structure in RS. In RSDZ, the absorption band at 744 cm^{-1} was associated with the symmetric stretching vibration of the Al-O bond in the zeolite structure Si-O-Al, while the absorption band at 606 cm^{-1} was related to the unique double six-ring structure in zeolite [34,35]. This evidence corroborated with the XRD results, confirming that zeolite products had been produced.

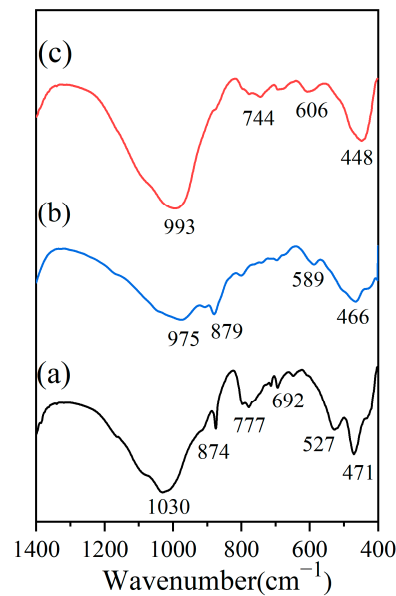


Figure 3. FT-IR spectra of RS (a), RSFP (b), and RSDZ (c).

3.2. Adsorption Properties in Single-Component Systems

3.2.1. Adsorption Isotherms

The adsorption isotherms of RSDZ for Zn^{2+} , Pb^{2+} , and Cu^{2+} in the single-component systems are shown in Figure 4. The adsorption isotherms were fitted using the Langmuir, Freundlich and D-R models. The results are shown in Table 2. The expressions for the Langmuir and Freundlich models are shown in the following Equations (4) and (5) [18]:

$$\frac{C_e}{q_e} = \frac{C_e}{q_{max}} + \frac{1}{k_L \times q_{max}} \quad (4)$$

$$\lg q_e = \frac{1}{n} \times \lg C_e + \lg K_F \quad (5)$$

where C_e is the equilibrium concentration ($\text{mmol}\cdot\text{L}^{-1}$), q_e is the equilibrium adsorption amount ($\text{mmol}\cdot\text{g}^{-1}$), K_L is the Langmuir constant, q_{max} is the maximum adsorption capacity given by the Langmuir model ($\text{mmol}\cdot\text{g}^{-1}$), and K_F is the Freundlich constant.

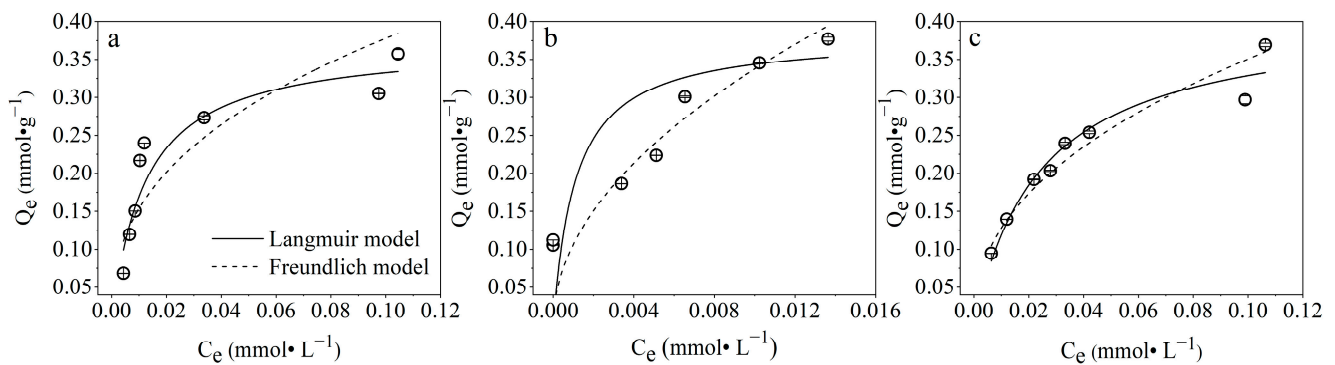


Figure 4. Adsorption isotherms of RSDZ for Zn^{2+} (a), Pb^{2+} (b), and Cu^{2+} (c).

Table 2. Fitting results of adsorption isotherms of RSDZ.

Heavy Metals	Langmuir Model			Freundlich Model			D-R Model	
	$K_L/(\text{L}\cdot\text{mmol}^{-1})$	$q_{max}/(\text{mmol}\cdot\text{g}^{-1})$	R^2	$K_F/(\text{mmol}\cdot\text{g}^{-1})\cdot(\text{mmol}\cdot\text{L}^{-1})^{-1/n}$	$1/n$	R^2	$E/(\text{kJ}\cdot\text{mol}^{-1})$	R^2
Zn^{2+}	81.93	0.37	0.979	0.92	0.390	0.742	12.91	0.769
Pb^{2+}	666.54	0.38	0.910	3.76	0.524	0.947	12.91	0.956
Cu^{2+}	41.05	0.40	0.965	0.96	0.437	0.9581	12.91	0.969

The expressions for the D-R model are shown in Equations (6)–(8) [36]:

$$q_e = q_{max} \exp(-K_D \varepsilon^2) \quad (6)$$

$$\varepsilon = RT \ln(1 + 1/C_e) \quad (7)$$

$$E = \frac{1}{(2K_D)^{0.5}} \quad (8)$$

where q_e and q_{max} (Equation (6)) are the equilibrium and maximum adsorption capacity, respectively ($\text{mol}\cdot\text{g}^{-1}$), K_D is the adsorption constant related to the mean free energy of the adsorption process ($\text{mol}^2\cdot\text{J}^{-2}$), ε is the adsorption potential ($\text{J}\cdot\text{mol}^{-1}$), R is the ideal gas constant $8.314 \text{ J}\cdot(\text{mol}\cdot\text{K})^{-1}$, T is the absolute temperature (K), C_e (Equation (7)) is the equilibrium concentration ($\text{mol}\cdot\text{L}^{-1}$), and E is the free energy of adsorption ($\text{kJ}\cdot\text{mol}^{-1}$).

As the equilibrium concentration increased, the adsorption capacity of RSDZ for Zn^{2+} , Pb^{2+} , and Cu^{2+} showed a trend of rapid increase, followed by a slow increase and finally reached saturation. This was because, at low concentrations, there were sufficient adsorption sites on the adsorbent for the reaction to proceed rapidly. As the adsorption capacity increased with increasing concentration, the number of sites on RSDZ decreased gradually, eventually reaching saturation [37]. The adsorption isotherms for Zn^{2+} , Pb^{2+} , and Cu^{2+} all fit the Langmuir model well, with correlation coefficients > 0.9 , whereas those for Zn^{2+} poorly fit the Freundlich model. The adsorption energies of RSDZ for Zn^{2+} , Pb^{2+} , and Cu^{2+} were calculated using the D-R model; all exceeded $8 \text{ kJ}\cdot\text{mol}^{-1}$, indicating that ion exchange was the mechanism underlying the adsorption of the three heavy metal ions by RSDZ [36].

In terms of adsorption capacity, the maximum Langmuir adsorption capacity of RSDZ for Zn^{2+} , Pb^{2+} , and Cu^{2+} was 0.37 , 0.38 , and $0.40 \text{ mmol}\cdot\text{g}^{-1}$, respectively, which corresponded to 0.74 , 0.76 , and $0.80 \text{ meq}\cdot\text{g}^{-1}$, respectively. Based on the results in Table 1, the CEC of RSDZ was $0.61 \text{ meq}\cdot\text{g}^{-1}$; the higher adsorption capacity for heavy metal ions here suggests that the adsorption of heavy metal ions by RSDZ may not be entirely dependent on the ion exchange mechanism. Although the maximum adsorption of the three heavy metal ions by RSDZ was similar, the adsorption affinity (expressed as K_L)

of the RSDZ showed a pattern of $Pb^{2+} \gg Zn^{2+} > Cu^{2+}$, similar to the results reported in previous studies comparing the adsorption affinities of zeolite-like minerals for heavy metal elements [9].

Table 3 shows the data of the comparison of the adsorption capacity of RSDZ for Zn^{2+} , Pb^{2+} , and Cu^{2+} with previously reported heavy metal adsorbents. The adsorption capacity of RSDZ for Zn^{2+} , Pb^{2+} , and Cu^{2+} was significantly higher than that for natural zeolites [10,38–40] and comparable to both modified and synthetic zeolites [37,41–43]. The findings indicate that RSDZ offers some advantages as a low-cost heavy metal adsorbent.

Table 3. Comparison of Zn^{2+} , Pb^{2+} , and Cu^{2+} adsorption performance between RSDZ and reported adsorbents.

Adsorbent	Langmuir Adsorption Maximum ($mmol \cdot g^{-1}$)			Reference
	Zn^{2+}	Pb^{2+}	Cu^{2+}	
RSDZ	0.37	0.38	0.40	This study
Iranian natural zeolite	-	0.03	0.07	[38]
Iron-coated Australian zeolite	0.10	0.05	0.15	[39]
Clinoptilolite	0.10	0.21	-	[10]
Erionite	0.10	0.26	-	[10]
Na-type zeolite	-	0.30	-	[40]
Lanthanum modified zeolite	0.27	-	-	[37]
Chitosan-zeolite composite	-	-	0.40	[41]
Synthetic-zeolite	-	0.32	0.88	[42]
Synthetic Na-clinoptilolite	0.48	0.88	0.53	[43]

3.2.2. Effect of Initial Solution pH

The initial solution pH is one of the most important factors affecting the effectiveness of heavy metal ion adsorption. Solution pH can alter the surface charge characteristics of the adsorbent and speciation of heavy metal ions, which in turn can affect the adsorption performance [37]. As the pH of heavy metal wastewater is generally acidic, the pH range examined in this experiment was 1–7. Figure 5 shows the adsorption performance of RSDZ on Pb^{2+} , Zn^{2+} , and Cu^{2+} under different initial pH conditions. The adsorption capacities for Pb^{2+} , Zn^{2+} , and Cu^{2+} increased sharply as pH increased from 1 to 3, reaching 0.43, 0.44 and $0.40 \text{ mmol} \cdot g^{-1}$ at pH 3, respectively. Subsequently, as solution pH continued to increase, the adsorption capacity of RSDZ for the three heavy metals essentially remained stable. These results were similar to the findings of previous studies [44,45] and were due to the protonation effect under strongly acidic conditions, which resulted in a large positive charge at the active site of the adsorbent, leading to strong electrostatic repulsion with the target heavy metal ion. In addition, large amounts of H_3O^+ and H^+ were present in the solution, which competed with the target ion for the adsorption site. Conversely, as the solution pH increased, the negative charge density on the surface of the material increased due to the deprotonation of the metal ion binding sites. Thus, the metal ions were able to effectively utilise the available binding sites through electrostatic attraction and complexation or form metal oxide precipitates, thereby improving the adsorption performance [37].

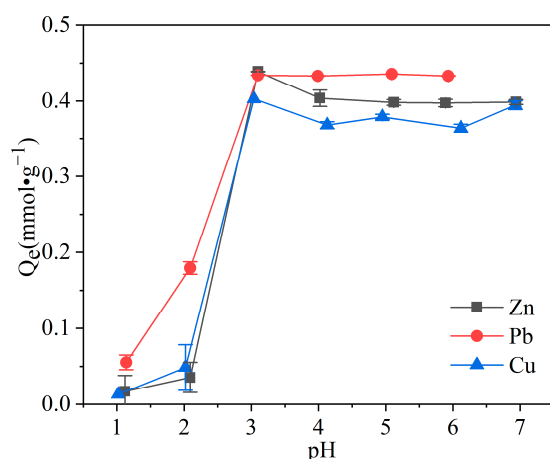


Figure 5. Effect of initial pH on adsorption performance by RSDZ.

3.3. Adsorption Performance under Multi-Component Competition

Actual heavy metal wastewater often simultaneously contains multiple metal ions, which may have mutual effects on their respective adsorption capacities when treated with zeolites. Therefore, multi-component competitive adsorption experiments were performed to clarify the adsorption performance of RSDZ for Zn^{2+} , Pb^{2+} , and Cu^{2+} under coexisting conditions and to elucidate their competition mechanism on the RSDZ surface.

3.3.1. Competitive Adsorption in Binary Systems

Figure 6 shows the changes in the adsorption performance of RSDZ for Zn^{2+} , Pb^{2+} , and Cu^{2+} with equilibrium concentration in the binary systems. In the Zn-Cu binary system, the adsorption capacity for Zn^{2+} and Cu^{2+} did not change significantly compared to that in the unary systems at low equilibrium concentrations (Figure 6a). This was because there were sufficient adsorption sites on the RSDZ surface at this point, and the coexistence of heavy metal ions had a limited mutual effect on their adsorption capacities. At high equilibrium concentrations, the coexistence of Zn^{2+} and Cu^{2+} resulted in a significant decrease in the adsorption capacity for both ions. The K_d values for Zn^{2+} were consistently greater than those for Cu^{2+} in the Zn-Cu binary system (Table 4), indicating that RSDZ was more selective for Zn^{2+} than for Cu^{2+} . Cu^{2+} and Pb^{2+} displayed significant competitive adsorption in the Pb-Cu binary system under all concentrations, and the distribution coefficient K_d of Pb^{2+} was also consistently greater than that of Cu^{2+} at all initial concentrations (Figure 6b and Table 4). These findings suggest that RSDZ has a higher selectivity for Pb^{2+} than Cu^{2+} . Adsorption of both Zn^{2+} and Pb^{2+} in the Zn-Pb binary system decreased to some extent compared to that in the unary systems (Figure 6c). Data of distribution coefficients K_d (Table 4) revealed a greater K_d for Zn^{2+} than that for Pb^{2+} when the initial concentration was $<0.3 \text{ mmol}\cdot\text{L}^{-1}$, whereas the K_d for Pb^{2+} was greater than that for Zn^{2+} when the concentration continued to rise above $0.4 \text{ mmol}\cdot\text{L}^{-1}$. These findings indicate that the selectivity of RSDZ for Zn^{2+} and Pb^{2+} was related to their initial concentrations. In general, RSDZ was more selective for the heavy metals Zn^{2+} and Pb^{2+} than Cu^{2+} in the binary system, whereas the selectivity between Zn^{2+} and Pb^{2+} was concentration-dependent.

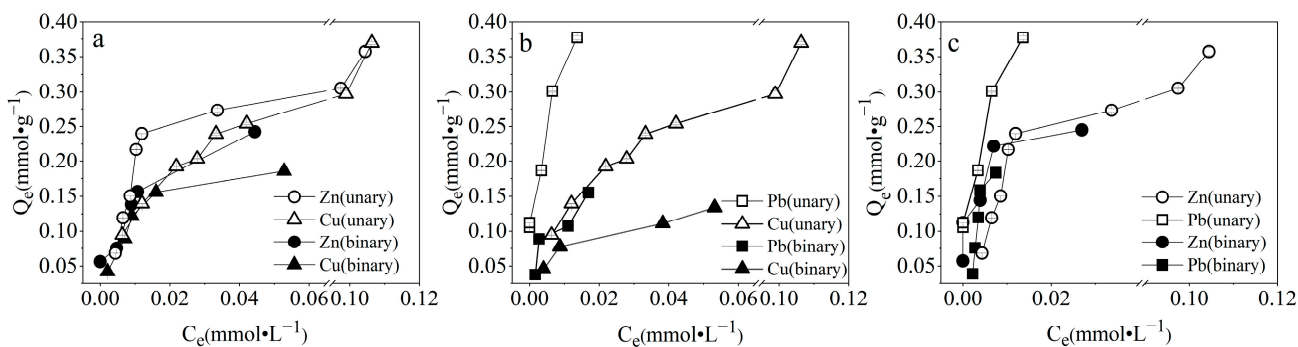


Figure 6. Adsorption amount by RSDZ versus equilibrium concentration in Cu-Zn (a), Cu-Pb (b), and Zn-Pb (c) binary systems.

Table 4. K_d values in binary systems at different initial heavy metal concentrations.

Systems	Heavy Metals	K_d ($L \cdot kg^{-1}$)				
		0.1 $mmol \cdot L^{-1}$	0.2 $mmol \cdot L^{-1}$	0.3 $mmol \cdot L^{-1}$	0.4 $mmol \cdot L^{-1}$	0.5 $mmol \cdot L^{-1}$
Zn-Cu	Cu^{2+}	20,238.10	12,637.43	13,342.83	9726.44	3511.93
	Zn^{2+}	- ¹	15,891.36	15,412.19	14,587.10	11,467.92
Cu-Pb	Cu^{2+}	11,381.15	8847.44	2906.36	2519.01	6093.82
	Pb^{2+}	22,903.35	32,326.21	9734.52	9171.02	18,023.09
Zn-Pb	Zn^{2+}	-	-	36,894.20	31,722.99	9082.29
	Pb^{2+}	17,701.93	27,519.16	34,120.07	40,521.55	24,523.01

¹ K_d value is infinity as equilibrium concentrations were 0.

3.3.2. Competitive Adsorption in the Ternary System

The changes in the adsorption performance of RSDZ for Zn^{2+} , Pb^{2+} , and Cu^{2+} with equilibrium concentration in the Zn-Pb-Cu ternary system are shown in Figure 7. The coexistence of heavy metal ions in the ternary system resulted in a substantial decrease in the adsorption amount for Zn^{2+} , Pb^{2+} , and Cu^{2+} compared to the unary systems, indicating the presence of competitive effects. The distribution coefficient (K_d) data (Table 5) revealed that in the ternary system, RSDZ had the lowest affinity for Cu^{2+} . Furthermore, at low initial concentrations, its affinity for Zn^{2+} was greater than that for Pb^{2+} , whereas the opposite pattern was observed at high initial concentrations. These findings agree with the conclusions based on the binary systems.

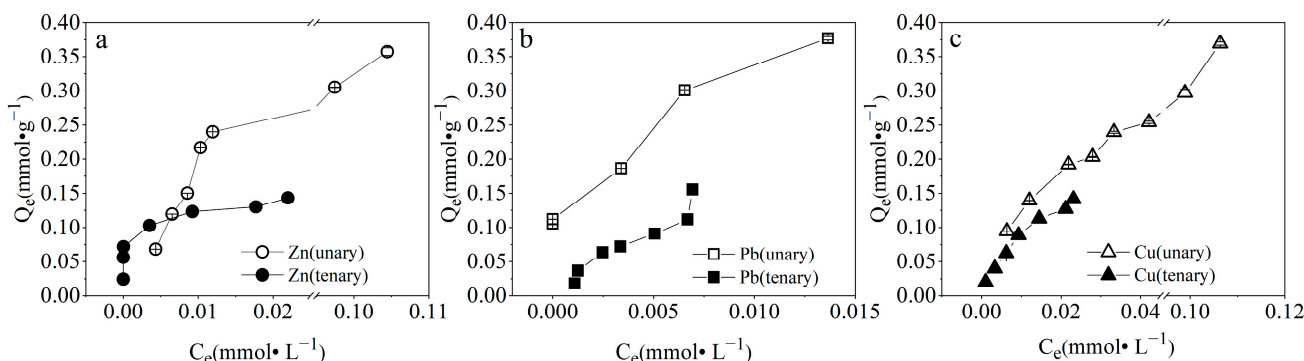


Figure 7. Adsorption amount of Zn^{2+} (a), Pb^{2+} (b), and Cu^{2+} (c) by RSDZ versus equilibrium concentration in ternary systems.

Table 5. K_d values in the ternary system at different initial heavy metal concentrations.

Heavy Metals	K_d (L·kg ⁻¹)						
	0.05 mmol·L ⁻¹	0.1 mmol·L ⁻¹	0.15 mmol·L ⁻¹	0.2 mmol·L ⁻¹	0.25 mmol·L ⁻¹	0.3 mmol·L ⁻¹	0.35 mmol·L ⁻¹
Cu ²⁺	19,635.29	11,987.84	10,086.01	9525.15	7798.27	6011.47	6066.04
Pb ²⁺	16,668.59	29,465.30	25,666.86	21,525.11	17,980.01	16,721.50	22,427.41
Zn ²⁺	- ¹	-	1,804,676.92	29,383.34	13,329.89	7354.30	6510.40

¹ K_d value is infinity as equilibrium concentrations were 0.

The competitive adsorption behaviour of heavy metal ions is related to their ionic radius, relative atomic weight and hydrolysis constant [25]. As can be seen from Table S1, Pb²⁺ had the largest ionic radius, largest relative atomic weight, and smallest pK_h value. Hence, RSDZ showed the strongest selectivity for Pb²⁺. These findings are also consistent with the results of previous studies on the order of heavy metal adsorption by zeolite-like minerals [9,46]. However, although Zn²⁺ had the most unfavourable pK_h value among the three metals for adsorption, its selectivity in the binary and ternary systems was still higher than that of Cu²⁺, which may be related to the larger ionic radius and relative atomic weight of Zn²⁺ than Cu²⁺. At lower initial concentrations, Zn²⁺ showed higher selectivity than Pb²⁺, whereas at higher initial concentrations, Pb²⁺ showed higher selectivity than Zn²⁺. Higher concentrations of pollutants can promote the occurrence of adsorption reactions. This phenomenon is termed the concentration effect [47]. The discrepancies in the selectivity for Pb²⁺ and Zn²⁺ at different concentration ranges may be due to discrepancies in the concentration effects of different heavy metals in the adsorption reaction.

3.4. Reusability

The reusability of adsorbent is important for its practical application. Therefore, a four-cycle adsorption-desorption experiment was performed. The results are shown in Table 6. The removal rate of Zn²⁺, Pb²⁺, and Cu²⁺ were constantly > 85% in the four cycles, indicating the attenuation of adsorption capacity for RSDZ was very limited. Thus, the adsorbent displayed satisfactory reusability.

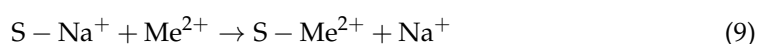
Table 6. Removal rate of heavy metal ions in adsorption-desorption experiment.

Cycle Number	Zn ²⁺	Pb ²⁺	Cu ²⁺
1	92.16%	99.30%	90.04%
2	91.36%	98.01%	91.02%
3	87.31%	92.53%	91.28%
4	85.26%	91.34%	88.37%

3.5. Adsorption Mechanisms

3.5.1. XPS Characterisation

Figure 8 shows the wide scan XPS spectra of RSDZ before and after the adsorption of Zn²⁺, Pb²⁺, and Cu²⁺. Na1s, O1s, NaKL1, Ca2p, C1s, Si2p, and Al2p peaks were detected on the RSDZ surface prior to adsorption. After the adsorption of heavy metals, new peaks appeared on the RSDZ surface. The adsorption of Zn²⁺, Pb²⁺, and Cu²⁺ was followed by the appearance of Zn2p, Pb4d, and Cu2p peaks. These findings indicate the successful adsorption of Zn²⁺, Pb²⁺, and Cu²⁺ on RSDZ. In addition, the peak intensities of Na1s and NaKL1 were significantly weaker compared to those before adsorption, which also suggests the occurrence of ion exchange between Na⁺ and Zn²⁺, Pb²⁺, or Cu²⁺ [48]. These findings are consistent with the results of the adsorption energy calculated in Section 2.2 using the D-R model. The reaction process of the ion exchange reaction is shown in Equation (9) [48]:



where S is the RSDZ surface and Me^{2+} represents Zn^{2+} , Pb^{2+} , and Cu^{2+} .

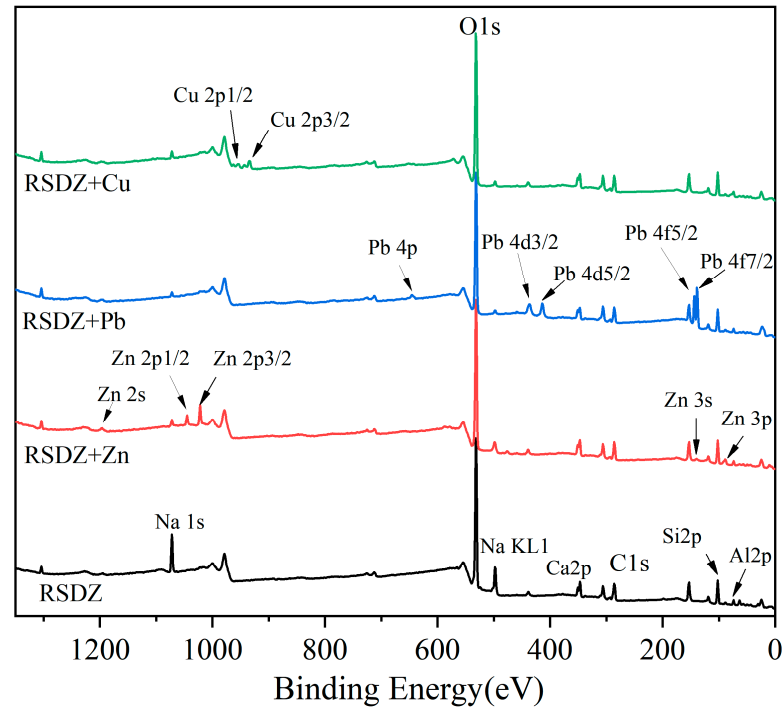


Figure 8. Wide scan XPS spectra of RSDZ before and after adsorption.

Figure 9 shows the XPS high-resolution spectra of the Si2p and Al2p orbitals before and after the adsorption of Zn^{2+} , Pb^{2+} , and Cu^{2+} by the RSDZ adsorbent. Only slight changes were observed in the Si2p and Al2p orbital binding energy of RSDZ after the adsorption of Zn^{2+} , Pb^{2+} , and Cu^{2+} , suggesting that the chemical reactions between RSDZ and Zn^{2+} , Pb^{2+} , and Cu^{2+} were relatively weak. Thus, the contribution of chemisorption to heavy metal removal by RSDZ may be relatively small.

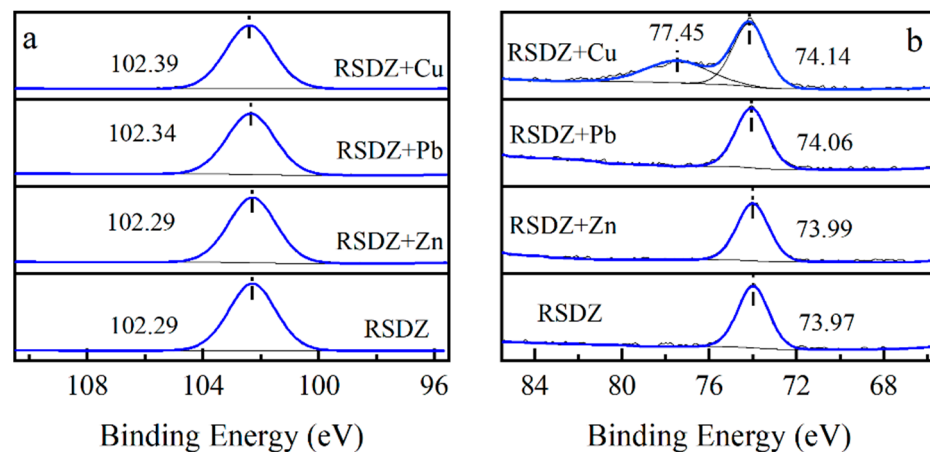


Figure 9. High-resolution Si 2p (a) and Al 2p (b) spectra of RSDZ before and after adsorption.

3.5.2. FT-IR Characterisation

FT-IR analysis was performed on RSDZ before and after adsorption to clarify whether a chemisorption mechanism was active in the adsorption of Zn^{2+} , Pb^{2+} , and Cu^{2+} by RSDZ. The results shown in Figure 10 reveal that after the adsorption of Zn^{2+} , Pb^{2+} , and Cu^{2+} , the existing peaks did not disappear, and no new peaks appeared. However, some peaks shifted their position. The characteristic peaks at 1636 and 3445 cm^{-1} in RSDZ are associated with the bending vibrations of the -OH group in the zeolite structure. The positions of both

peaks had shifted after adsorption, suggesting that the -OH group had been transformed into an -O-Me group (where Me represents the Zn, Pb, and Cu atoms) [49]. Furthermore, the RSDZ peak at 744 cm^{-1} decreased to 737 , 739 , and 727 cm^{-1} , respectively, after the adsorption reaction, which also confirms that the -OH groups attached to the Al atoms in the zeolite structure are involved in the heavy metal removal process. The chemisorption reaction involving the hydroxyl -OH on the RSDZ surface can be expressed as Equation (10) [50]:



where X represents Si and Al atoms on the RSDZ surface.

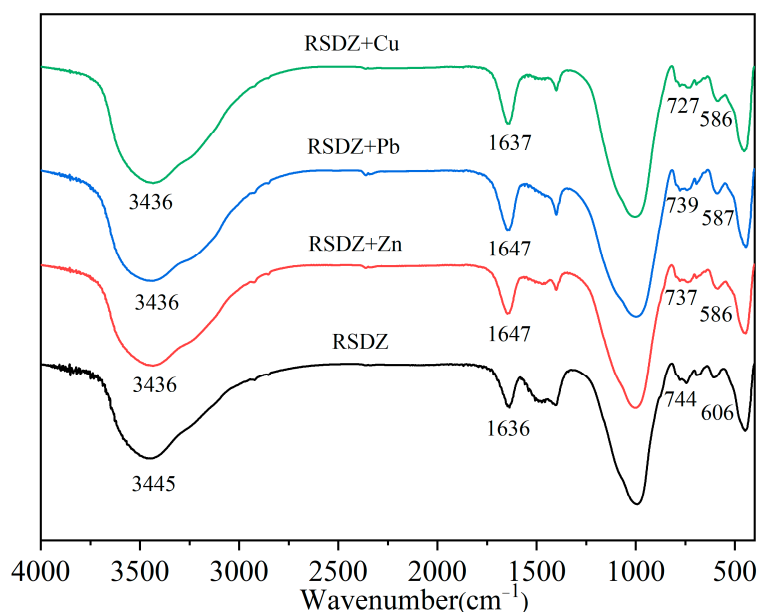


Figure 10. FT-IR spectra of RSDZ before and after adsorption.

3.5.3. Proposed Adsorption Mechanism

Combining the results of XPS and FT-IR spectra, it could be concluded that the adsorption of Zn^{2+} , Pb^{2+} , and Cu^{2+} by RSDZ was mainly due to the exchange of Na^+ on the RSDZ surface by the heavy metal ions. However, the chemisorption reaction involving the hydroxyl -OH on the RSDZ surface also contributes to the heavy metal ion removal, although its effect seems to be relatively low.

3.6. Economic Feasibility of RSDZ

Finally, to investigate the economic feasibility of RSDZ, a cost analysis was performed according to the results of the laboratory experiment. The cost of RSDZ was 3.18 Renminbi (RMB) per kilogram. Compared with the price of natural clinoptilolite ($1\text{ RMB}\cdot\text{kg}^{-1}$), RSDZ seems to be more expensive. However, judging from the view of the cost-performance ratio, RSDZ might be better as its Langmuir adsorption maximum for Zn^{2+} ($0.37\text{ mmol}\cdot\text{g}^{-1}$) was more than three times larger than that of natural clinoptilolite (see details in Table 3). Additionally, the cost could be further lowered when RSDZ was further promoted to the industrialised stage. Therefore, RSDZ is economically feasible as a novel adsorbent.

3.7. Limitation and Outlook

The chemical composition of raw material would influence the characteristics of the synthesised zeolite. For example, Yu reported that changes in the Si/Al molar ratios of raw material might alter the acidity, pore structure and surface morphology of zeolite product [51]. Therefore, the microscopic structure and heavy metal adsorption capability of

RSDZ might be uncertain when components of RS are variable. In our future research, the effect of the chemical composition of RS on the properties of RSDZ should be further evaluated.

4. Conclusions

The aluminosilicate-containing minerals in RS were transformed into NaP1 zeolites via a fusion-hydrothermal reaction to yield the product RSDZ. The maximum adsorption capacity of RSDZ for Zn^{2+} , Pb^{2+} , and Cu^{2+} was 0.37, 0.38, and 0.40 $mmol \cdot g^{-1}$, respectively. Both in binary and ternary systems, RSDZ showed a much greater affinity for Zn^{2+} and Pb^{2+} than for Cu^{2+} . However, the relative affinity of RSDZ for Pb^{2+} and Zn^{2+} was influenced by their concentration, with higher affinity of Pb^{2+} concentration $> 0.4 mmol \cdot L^{-1}$ in binary systems and $> 0.25 mmol \cdot L^{-1}$ in ternary systems. XPS and FT-IR characterisation revealed that the adsorption mechanism mainly involved ion exchange between heavy metal ions and Na^+ on the RSDZ surface, accompanied by a ligand exchange mechanism involving Si/Al linked -OH groups.

Supplementary Materials: The following supporting information can be downloaded at <https://www.mdpi.com/article/10.3390/su151813515/s1>, Figure S1: N_2 adsorption isotherms of RS and RSDZ; Table S1: Basic properties of Zn^{2+} , Pb^{2+} and Cu^{2+} [1].

Author Contributions: Conceptualization, Z.W.; methodology, Z.W.; validation, Y.Z. and L.W.; investigation, W.L.; writing—original draft preparation, Z.W. and W.L.; writing—review and editing, Z.W.; supervision, Y.L. and J.L.; funding acquisition, Y.L. All authors have read and agreed to the published version of the manuscript.

Funding: This research was funded by National Natural Science Foundation of China (grant number: 51909210), Chinese Postdoctoral Science Foundation (grant number: 2018M633648XB), Shaanxi Postdoctoral Science Foundation (grant number: 2018BSHYDZZ19), “Scientists+Engineers” Team Construction Based on QinChuangYuan Platform, Shaanxi Province (grant number: No. 2022KXJ-115).

Institutional Review Board Statement: Not applicable.

Informed Consent Statement: Not applicable.

Data Availability Statement: Not applicable.

Conflicts of Interest: The authors declare no conflict of interest.

References

1. Wu, Y.; Li, X.; Yu, L.; Wang, T.; Wang, J.; Liu, T. Review of soil heavy metal pollution in China: Spatial distribution, primary sources, and remediation alternatives. *Resour. Conserv. Recycl.* **2022**, *181*, 106261. [[CrossRef](#)]
2. Li, Q.; Liu, G.; Qi, L.; Wang, H.; Ye, Z.; Zhao, Q. Heavy metal-contained wastewater in China: Discharge, management and treatment. *Sci. Total Environ.* **2022**, *808*, 152091. [[CrossRef](#)] [[PubMed](#)]
3. Yu, Y.; He, J.; Sun, J.; Pei, Z.; Wu, Q.; Yu, R. Capacity and mechanisms of Pb(II) and Cd(II) sorption on five plant-based biochars. *Sustainability* **2023**, *15*, 7627. [[CrossRef](#)]
4. Fei, Y.; Hu, Y. Recent progress in removal of heavy metals from wastewater: A comprehensive review. *Chemosphere* **2023**, *335*, 139077. [[CrossRef](#)]
5. Chen, X.; Hossain, M.F.; Duan, C.; Liu, J.; Tsang, Y.F.; Islam, M.S.; Zhou, Y. Isotherm models for adsorption of heavy metals from water—A review. *Chemosphere* **2022**, *307*, 135545. [[CrossRef](#)]
6. Muhammad, A.N.; Tayyaba, N.; Khurram, S.; Muhammad, A.W.; Tajamal, H.; Muhammad, K.T.; Syed SA, S.; Azizur, R. Heterointerface engineering of water stable ZIF-8@ZIF-67: Adsorption of rhodamine B from water. *Surf. Interfaces* **2022**, *34*, 102324.
7. Muhammad, A.N.; Tayyaba, N.; Shazia, J.; Muhammad, A.W.; Muhammad, S.B.; Syed SA, S.; Azizur, R. Facile synthesis of Tri-metallic layered double hydroxides (NiZnAl-LDHs): Adsorption of Rhodamine-B and methyl orange from water. *Inorg. Chem. Commun.* **2022**, *145*, 110008.
8. Velarde, L.; Nabavi, M.S.; Escalera, E.; Antti, M.; Ahkter, F. Adsorption of heavy metals on natural zeolites: A review. *Chemosphere* **2023**, *328*, 138508. [[CrossRef](#)]
9. Erdem, E.; Karapinar, N.; Donat, R. The removal of heavy metal cations by natural zeolites. *J. Colloid Interface Sci.* **2004**, *280*, 309–314. [[CrossRef](#)]
10. Hernández-Montoya, V.; Pérez-Cruz, M.A.; Mendoza-CastilloSD, I.; Moreno-Virgen, M.R.; Bonilla-Petriciolet, A. Competitive adsorption of dyes and heavy metals on zeolitic structures. *J. Environ. Manag.* **2013**, *116*, 213–221. [[CrossRef](#)]

11. Bai, M.; Xiao, J.; Gao, Q.; Shen, J. Utilization of construction spoil and recycled powder in fired bricks. *Case Stud. Constr. Mater.* **2023**, *18*, e02024. [[CrossRef](#)]
12. Santha Kumar, G.; Saine, P.; Deoliya, R.; Mishra, A.K.; Negi, S.K. Characterization of laterite soil and its use in construction applications: A review. *Resour. Conserv. Recycl. Adv.* **2022**, *16*, 200120. [[CrossRef](#)]
13. Lou, Y.; Gao, Z.; Sun, G.; Wu, T.; Zhou, F.; Ai, J.; Cen, Y.; Xie, J. Runoff scouring experimental study of rill erosion of spoil tips. *Catena* **2022**, *214*, 106249. [[CrossRef](#)]
14. Wu, H.; Yao, P.; Yang, D.; Wang, C.; Shen, J.; Ma, Z. Upcycling of construction spoil powder as partial cement replacement for sustainable cement-based materials: Properties and modification. *J. Clean. Prod.* **2022**, *369*, 133361. [[CrossRef](#)]
15. Hou, Y.; Xiao, J.; Shen, J.; Gao, Q. Effects of distiller's grains and seawater on properties of sintered brick made from construction spoil. *J. Build. Eng.* **2022**, *62*, 105391. [[CrossRef](#)]
16. Jian, S.; Cheng, C.; Lv, Y.; Wang, C.; Tan, H.; Li, B. Preparation and evaluation of high-fluid backfill materials from construction spoil. *Constr. Build. Mater.* **2022**, *345*, 128370. [[CrossRef](#)]
17. Rydgren, K.; Halvorsen, R.; Odlang, A.; Skjerdal, G. Restoration of alpine spoil heaps: Successional rates predict vegetation recovery in 50 years. *Ecol. Eng.* **2011**, *37*, 294–301. [[CrossRef](#)]
18. Chu, D.; Amar, M.; Benzerzour, M.; Kleib, J.; Abriak, N. Flash-calcined sediments for zinc adsorption. *Sustainability* **2023**, *15*, 10230. [[CrossRef](#)]
19. Wang, C.; Zhou, J.; Wang, Y.; Yang, M.; Li, Y.; Meng, C. Synthesis of zeolite X from low-grade bauxite. *J. Chem. Technol. Biotechnol.* **2013**, *88*, 1350–1357. [[CrossRef](#)]
20. Garcia, G.; Cardenas, E.; Cabrera, S.; Hedlund, J.; Mouzon, J. Synthesis of zeolite Y from diatomite as silica source. *Microporous Mesoporous Mater.* **2016**, *219*, 29–37. [[CrossRef](#)]
21. Wu, Z.; Chen, T.; Liu, H.; Wang, C.; Cheng, P.; Chen, D.; Xie, J. An insight into the comprehensive application of opal-palygorskite clay: Synthesis of 4A zeolite and uptake of Hg²⁺. *Appl. Clay Sci.* **2018**, *165*, 103–111. [[CrossRef](#)]
22. Yang, J.; Liu, H.; Diao, H.; Li, B.; Yue, Y.; Bao, X. A Quasi-solid-phase approach to activate natural minerals for zeolite synthesis. *Acs Sustain. Chem. Eng.* **2017**, *5*, 3233–3242. [[CrossRef](#)]
23. Liu, H.; Shen, T.; Li, T.; Yuan, P.; Shi, G.; Bao, X. Green synthesis of zeolites from a natural aluminosilicate mineral rectorite: Effects of thermal treatment temperature. *Appl. Clay Sci.* **2014**, *90*, 53–60. [[CrossRef](#)]
24. Kazak, E.; Kazak, A. Experimental features of cation exchange capacity determination in organic-rich mudstones. *J. Nat. Gas Sci. Eng.* **2020**, *83*, 103456. [[CrossRef](#)]
25. Park, J.; Ok, Y.; Kim, S.; Cho, J.; Heo, J.; Delaune, R.D.; Seo, D. Competitive adsorption of heavy metals onto sesame straw biochar in aqueous solutions. *Chemosphere* **2016**, *142*, 77–83. [[CrossRef](#)]
26. Belviso, C. State-of-the-art applications of fly ash from coal and biomass: A focus on zeolite synthesis processes and issues. *Prog. Energy Combust. Sci.* **2018**, *65*, 109–135. [[CrossRef](#)]
27. Cheng, Y.; Xu, L.; Liu, C. NaP1 zeolite synthesized via effective extraction of Si and Al from red mud for methylene blue adsorption. *Adv. Powder Technol.* **2021**, *32*, 3904–3914. [[CrossRef](#)]
28. Wang, Z.; Fan, Y.; Li, Y.; Qu, F.; Wu, D.; Kong, H. Synthesis of zeolite/hydrous lanthanum oxide composite from coal fly ash for efficient phosphate removal from lake water. *Microporous Mesoporous Mater.* **2016**, *222*, 226–234. [[CrossRef](#)]
29. Wu, D.; Lu, Y.; Kong, H.; Ye, C.; Jin, X. Synthesis of zeolite from thermally treated sediment. *Ind. Eng. Chem. Res.* **2008**, *47*, 295–302. [[CrossRef](#)]
30. Chen, Q.; Zhao, Y.; Qiu, Q.; Long, L.; Liu, X.; Lin, S.; Jiang, X. Zeolite NaP1 synthesized from municipal solid waste incineration fly ash for photocatalytic degradation of methylene blue. *Environ. Res.* **2023**, *218*, 114873. [[CrossRef](#)]
31. Tanaka, H.; Furusawa, S.; Hino, R. Synthesis, characterization, and formation process of Na-X zeolite from coal fly ash. *J. Mater. Synth. Process.* **2002**, *10*, 143–148. [[CrossRef](#)]
32. Tanaka, H.; Miyagawa, A.; Eguchi, H.; Hino, R. Synthesis of a single-phase Na-A zeolite from coal fly ash by dialysis. *Ind. Eng. Chem. Res.* **2004**, *43*, 6090–6094. [[CrossRef](#)]
33. Zhao, H.; Deng, Y.; Harsh, J.; Flury, H.M.; Boyle, J.S. Alteration of kaolinite to cancrinite and sodalite by simulated Hanford tank waste and its impact on cesium retention. *Clays Clay Miner.* **2004**, *52*, 1–13. [[CrossRef](#)]
34. Mouhtaros, T.; Charistos, D.; Kantiranis, N.; Filippidis, A.; Kassoli-Fournaraki, A.; Tsirambidis, A. GIS-type zeolite synthesis from Greek lignite sulphocalcic fly ashes promoted by NaOH solutions. *Microporous Mesoporous Mater.* **2003**, *61*, 57–67. [[CrossRef](#)]
35. Ojha, K.; Pradhan, N.; Samanta, A. Zeolite from fly ash: Synthesis and characterization. *Bull. Mater. Sci.* **2004**, *27*, 555–564. [[CrossRef](#)]
36. Puccia, V.; Avena, M. On the use of the Dubinin-Radushkevich equation to distinguish between physical and chemical adsorption at the solid-water interface. *Colloid Interface Sci. Commun.* **2021**, *41*, 100376. [[CrossRef](#)]
37. Wang, Z.; Li, W.; Zhu, J.; Wang, D.; Meng, H.; Wang, H.; Li, J. Simultaneous adsorption of phosphate and zinc by lanthanum modified zeolite. *Environ. Technol. Innov.* **2021**, *24*, 101906. [[CrossRef](#)]
38. Merrikhpour, H.; Jalali, M. Comparative and competitive adsorption of cadmium, copper, nickel, and lead ions by Iranian natural zeolite. *Clean Technol. Environ. Policy* **2013**, *15*, 303–316. [[CrossRef](#)]
39. Nguyen, T.; Loganathan, P.; Nguyen, T.; Vigneswara, S.; Kandasamy, J.; Naidu, R. Simultaneous adsorption of Cd, Cr, Cu, Pb, and Zn by an iron-coated Australian zeolite in batch and fixed-bed column studies. *Chem. Eng. J.* **2015**, *270*, 393–404. [[CrossRef](#)]

40. Lv, B.; Deng, X.; Jiao, F.; Dong, B.; Fang, C.; Xing, B. Removal of Pb^{2+} in aqueous solutions using Na-type zeolite synthesized from coal gasification slag in a fluidized bed: Hydrodynamic and adsorption. *Process Saf. Environ. Prot.* **2023**, *174*, 869–881. [[CrossRef](#)]
41. Wan Ngah, W.; Teong, L.; Toh, R.; Hanafiah, M.A.K.M. Comparative study on adsorption and desorption of Cu(II) ions by three types of chitosan–zeolite composites. *Chem. Eng. J.* **2013**, *223*, 231–238. [[CrossRef](#)]
42. He, K.; Chen, Y.; Tang, Z.; Hu, Y. Removal of heavy metal ions from aqueous solution by zeolite synthesized from fly ash. *Environ. Sci. Pollut. Res.* **2016**, *23*, 2778–2788. [[CrossRef](#)] [[PubMed](#)]
43. Li, Y.; Bai, P.; Yan, Y.; Yan, W.; Shi, W.; Xu, R. Removal of Zn^{2+} , Pb^{2+} , Cd^{2+} , and Cu^{2+} from aqueous solution by synthetic clinoptilolite. *Microporous Mesoporous Mater.* **2019**, *273*, 203–211. [[CrossRef](#)]
44. Bashir, A.; Manzoor, T.; Malik, L.; Qureshi, A.; Pandith, A.H. Enhanced and selective adsorption of Zn(II), Pb(II), Cd(II), and Hg(II) Ions by a dumbbell- and flower-shaped potato starch phosphate polymer: A combined experimental and DFT calculation study. *ACS Omega* **2020**, *5*, 4853–4867. [[CrossRef](#)] [[PubMed](#)]
45. Kenawy, I.; Hafez, M.; Ismail, M.; Hashem, M.A. Adsorption of Cu(II), Cd(II), Hg(II), Pb(II) and Zn(II) from aqueous single metal solutions by guanyl-modified cellulose. *Int. J. Biol. Macromol.* **2018**, *107*, 1538–1549. [[CrossRef](#)] [[PubMed](#)]
46. Ouki, S.; Kavannagh, M. Treatment of metals-contaminated wastewaters by use of natural zeolites. *Water Sci. Technol.* **1999**, *39*, 115–122. [[CrossRef](#)]
47. Guan, Q.; Wu, D.; Lin, Y.; Chen, X.; Wang, X.; Li, C.; He, S.; Kong, H. Application of zeolitic material synthesized from thermally treated sediment to the removal of trivalent chromium from wastewater. *J. Hazard. Mater.* **2009**, *167*, 244–249. [[CrossRef](#)]
48. Zhan, Y.; Zhang, H.; Lin, J.; Zhang, Z.; Gao, J. Role of zeolite's exchangeable cations in phosphate adsorption onto zirconium-modified zeolite. *J. Mol. Liq.* **2017**, *243*, 624–637. [[CrossRef](#)]
49. Yurekli, Y. Determination of adsorption characteristics of synthetic NaX nanoparticles. *J. Hazard. Mater.* **2019**, *378*, 120743. [[CrossRef](#)]
50. Chen, M.; Nong, S.; Zhao, Y.; Riaz, M.S.; Xiao, Y.; Molokeev, M.S.; Haung, F. Renewable P-type zeolite for superior absorption of heavy metals: Isotherms, kinetics, and mechanism. *Sci. Total Environ.* **2020**, *726*, 138535. [[CrossRef](#)]
51. Yu, L.; Xu, C.; Zhang, W.; Zhou, Q.; Fu, X.; Liang, Y.; Guo, Z.; Wang, W. Tailoring the pore structure, morphology and acidity of MFI zeolites by the regulation of Si/Al ratio in the synthetic gel. *J. Solid State Chem.* **2023**, *327*, 124271. [[CrossRef](#)]

Disclaimer/Publisher's Note: The statements, opinions and data contained in all publications are solely those of the individual author(s) and contributor(s) and not of MDPI and/or the editor(s). MDPI and/or the editor(s) disclaim responsibility for any injury to people or property resulting from any ideas, methods, instructions or products referred to in the content.